

pubs.acs.org/NanoLett Letter

Observation of Room Temperature Exciton Polariton Emission from Wide Ranging 2D Semiconductors Coupled with a Broadband Mie Resonator

Jie Fang, Kan Yao, Mingsong Wang, Zhuohang Yu, Tianyi Zhang, Taizhi Jiang, Suichu Huang, Brian A. Korgel, Mauricio Terrones, Andrea Alu, and Yuebing Zheng



Cite This: Nano Lett. 2023. 23. 9803-9810



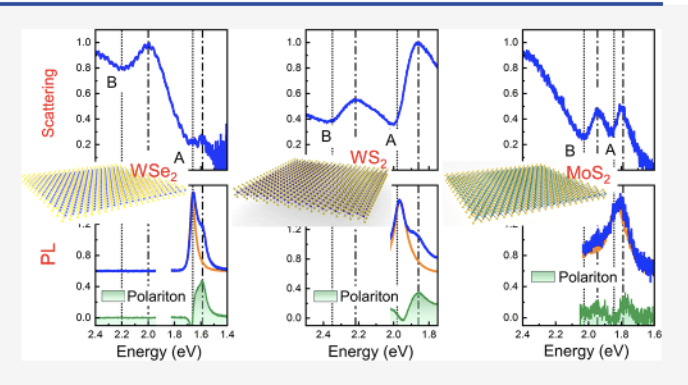
ACCESS I

III Metrics & More

Article Recommendations

Supporting Information

ABSTRACT: Two-dimensional exciton-polaritons in monolayer transition metal dichalcogenides (TMDs) exhibit practical advantages in valley coherence, optical nonlinearities, and even bosonic condensation owing to their light-emission capability. To achieve robust exciton-polariton emission, strong photon-exciton couplings are required at the TMD monolayer, which is challenging due to its atomic thickness. High-quality (Q) factor optical cavities with narrowband resonances are an effective approach but typically limited to a specific excitonic state of a certain TMD material. Herein, we achieve on-demand exciton-polariton emission from a wide range of TMDs at room temperature by hybridizing excitons with broadband Mie resonances spanning the whole visible spectrum. By confining



broadband light at the TMD monolayer, our one type of Mie resonator on different TMDs enables enhanced light-matter interactions with multiple excitonic states simultaneously. We demonstrate multi-Rabi splittings and robust polaritonic photoluminescence in monolayer WSe₂, WS₂, and MoS₂. The hybrid system also shows the potential to approach the ultrastrong coupling regime.

KEYWORDS: exciton-polariton emission. strong coupling. moderate refractive index. Mie resonances. monolayer transition metal dichalcogenides

onolayer transition metal dichalcogenides (TMDs) have emerged as a compelling platform for studying cavity quantum electrodynamics (QED) in the strong coupling (SC) regime at room temperature. 1,2 One major feature of SC is the formation of new exciton-polaritonic states when the coherent energy exchange between excitonic states and optical resonant modes is faster than the decoherence rate of the hybrid system.^{1,3} Specifically, two-dimensional (2D) TMD polaritons are promising for next-generation polaritonic devices because of their efficient polariton emission, 2,4-12 rich excitonic states spreading over the full visible regime, 1,13 and the efficient tunability of the excitonic properties, both electrically and optically. 13,14 In addition, Dufferwiel et al. reported that TMD polariton emissions are valley-addressable beyond intrinsic excitons. 10 Anton-Solanas et al. demonstrated bosonic condensation in TMD polaritons for spontaneous coherent light emission. ¹² All these exciting findings have triggered the demand for a universal SC platform for robust exciton-polariton emission in TMDs, which should not only be a proof-of-concept configuration for a specific excitonic state but instead present a full-visible-range coverage toward practical applications of the 2D TMD family.

In order to achieve SC and polariton emission, not only a high oscillator strength in excitonic materials but also enhanced optical fields via resonant cavities are required. High-Q cavity modes with diffuse mode volumes^{3,7,1,5} are commonly employed, taking advantage of a slower decoherence rate of the hybrid system.^{2,4–9} But the narrow line width of high-Q resonances limits their applicability, given the rich excitonic family in various TMD materials. Toward a broadband SC platform but with a lower Q_j reducing the mode volume can be an offset for stronger photon-exciton coupling. Thus, highly localized plasmonic modes in metallic nanostructures can be a candidate approach.^{2,5} Nevertheless, this solution inevitably introduces significant material loss, which is unwanted for efficient exciton-polariton radiations.

Received: July 7, 2023 Revised: October 18, 2023

Accepted: October 19, 2023 Published: October 25, 2023





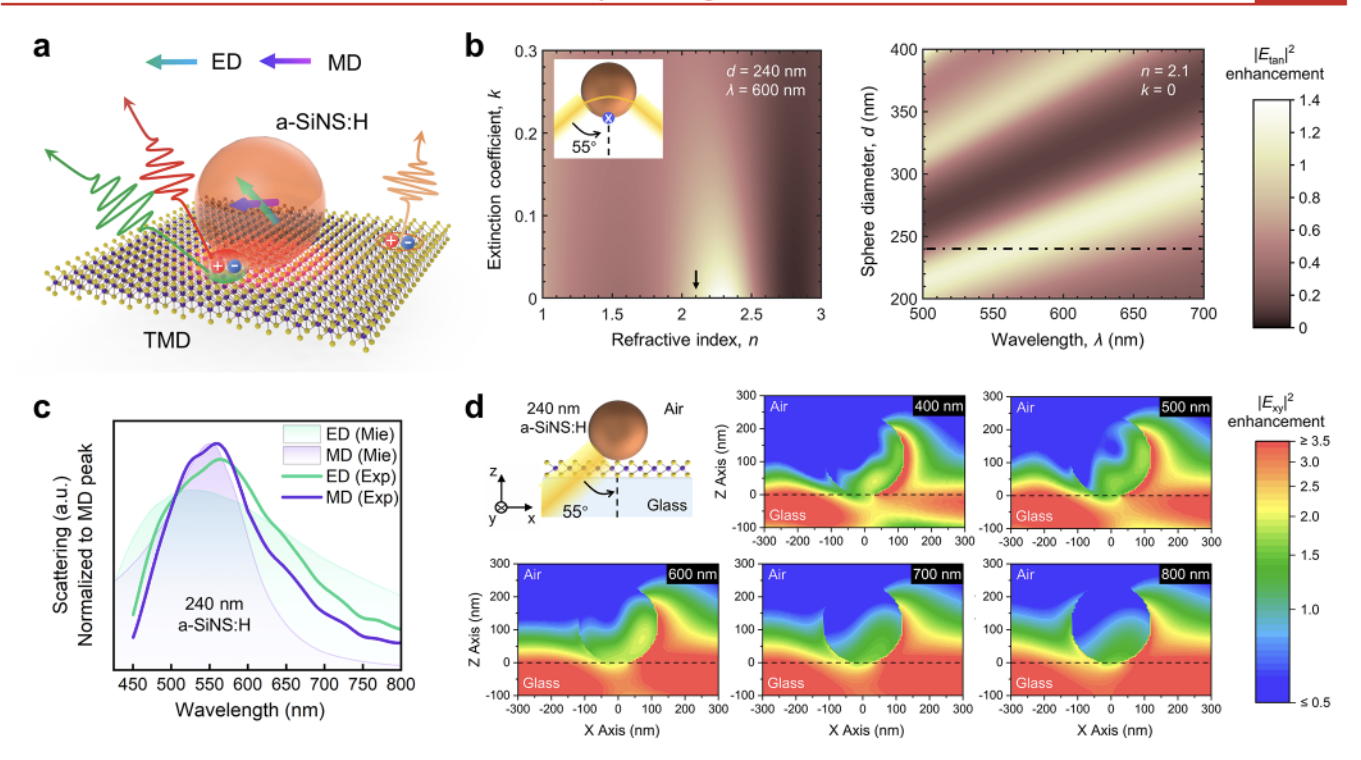


Figure 1. Broadband field enhancement localized at the TMD monolayer using an MRI Mie resonator. (a) Schematic of an a-SiNS:H nanoresonator on a TMD monolayer, leading to broadband strong coupling and robust exciton-polariton emission: ED (MD), electric (magnetic) dipole mode. (b) Analytically calculated mappings of the tangential field intensity ($|E_{\rm tan}|^2$) enhancement at one single spot on the nanosphere surface, with different material refractive indices n and absorption coefficients k when the sphere diameter d=240 nm and wavelength $\lambda=600$ nm (left) and with different d and λ when n=2.1 and k=0 (right). The arrow and dash-dotted line highlight n, k, and d of the a-SiNS:H under study. Inset: The blue dot with a cross is where the field enhancement is evaluated. A center-symmetric 55° oblique incident light is considered. Details of analysis can be found in Figure S1. (c) Spectrally overlapped ED and MD of a 240 nm a-SiNS:H, covering the visible wavelengths. The shaded peaks are derived from Mie theory, and the thick curves are measured by polarization-resolved scattering spectroscopy. (d) Simulated in-plane field ($|E_{xy}|^2$) enhancement profiles for a system consisting of a 240 nm a-SiNS:H on a glass substrate, excited by a 55° oblique incident light at different wavelengths (see the schematic at the top left).

Recently, Mie resonances in high-refractive-index dielectric materials have attracted great attention in nanophotonics because of the subwavelength optical field confinement and ultralow loss. These merits lead to the possibility of a broadband SC system involving Mie-type cavities and 2D TMDs; These merits lead to the possibility of a broadband SC system involving Mie-type cavities and 2D TMDs; The however, no exciton-polariton emission has been observed so far in such a system, Specially due to the limited spatial overlap between the TMD monolayer and the Mie modes mostly residing inside the dielectric nanostructures.

Herein, we propose a route to fully utilizing the advantages of Mie resonances in QED studies by introducing a moderate-refractive-index (MRI) Mie resonator coupled to monolayer TMDs. An MRI Mie resonator features more interactions between electric (ED) and magnetic dipole (MD) modes than its high-index counterpart. Therefore, through a rational design of the ED and MD of MRI Mie resonators, ²⁴ on-demand optical field manipulation can be achieved. ^{25,26} In this work, by tailoring the dielectric function and resonator size, we design single Mie resonators, i.e., hydrogenated amorphous silicon nanospheres (a-SiNS:Hs), ²⁷ specifically for broadband field enhancement localized at the atomically thin TMD monolayer (Figure 1a).

The tailored MRI Mie resonator serves as a broadband SC platform for a wide range of excitonic states in various TMD materials. Robust polariton photoluminescence (PL) and multiple Rabi splittings originating from the coupling with A, B, and C excitons are demonstrated in monolayer WSe₂, WS₂,

and MoS₂ at room temperature. Excitingly, the hybrid system shows the potential to approach the ultrastrong coupling (USC) regime, in which the coupling strength g and the exciton transition energy ω_0 are comparable. As a demo application based on our platform, excitation-wavelength-dependent PL spectroscopy is implemented to explore the radiative/nonradiative decay properties of different TMD exciton-polaritons, providing new insights into the development of active polaritonic devices.

To start with the design of our MRI Mie resonator, we first evaluate the field enhancement at one single spot on the surface of a free-standing a-SiNS:H as shown in Figure 1b. Enhanced optical fields at the surface, rather than inside the nanosphere, would allow for better spatial overlap with TMDs (Figure 1a). Since the bright exciton dipole moments in 2D TMDs are constrained in the monolayer plane, only the tangential electric field is considered. Mie theory is applied to quickly assess the field enhancement by running through all the parameters. Details can be found in Figure S1 and Section S3 in Supporting Information. By controlling the synthesis conditions (see Materials and Methods), our a-SiNS:Hs can be tuned in refractive index n, absorption coefficient k, and sphere diameter d. As shown in the left panel of Figure 1b, by sweeping n, k at a fixed d (240 nm), and wavelength λ (600 nm), we find a maximum enhancement when a moderate n of ~2.2 is accompanied by a vanishing k. Experimentally, a-SiNS:Hs with an n of ~ 2.1 and negligible k (see Supporting Information Section S1) are used. Then, with fixed n and k, the

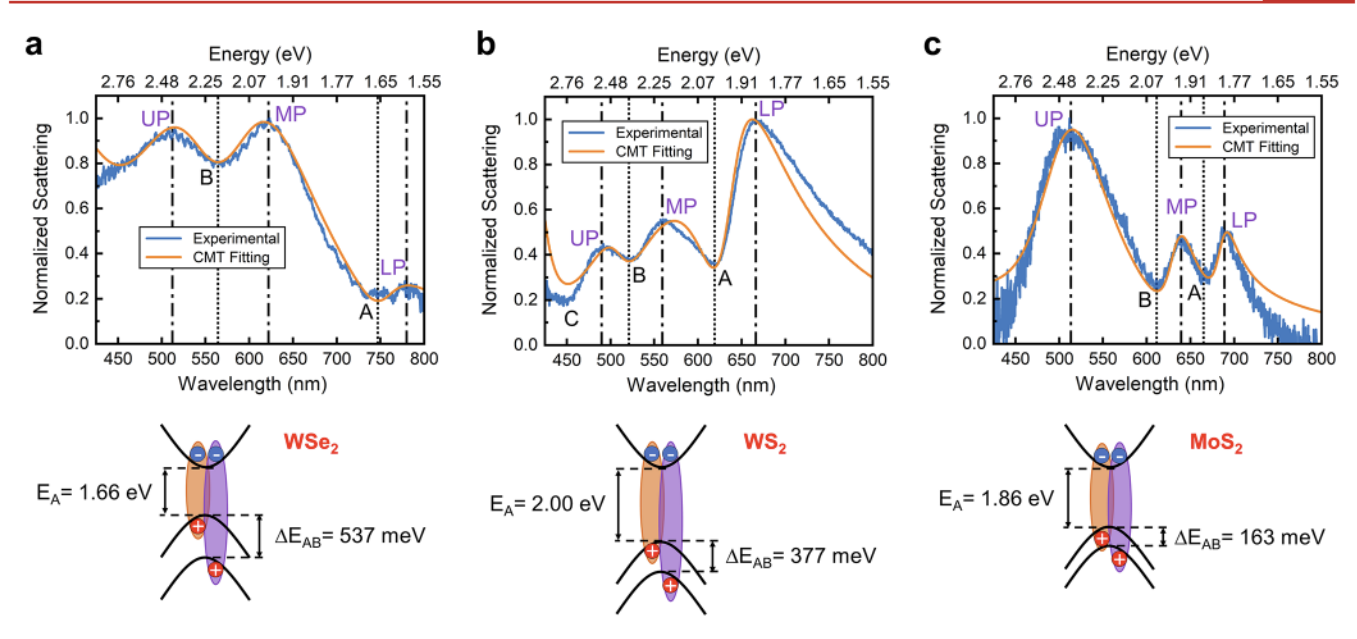


Figure 2. Multi-Rabi splittings and broadband enhanced light-matter interactions approaching the ultrastrong coupling (USC) regime in single a-SiNS:Hs on different TMD monolayers. (a–c) Top: Experimental single-particle scattering spectra and coupled mode theory (CMT) fittings with USC corrections for (a) WSe₂, (b) WSe₂, and (c) MoS₂ samples, respectively. The dotted lines mark the A, B, and C excitons, and the dash-dotted lines highlight the lower (LP), middle (MP), and upper (UP) exciton-polaritons. Bottom: Schematics showing the A (orange) and B (purple) exciton energy band structures and their energy difference ΔE_{AB} .

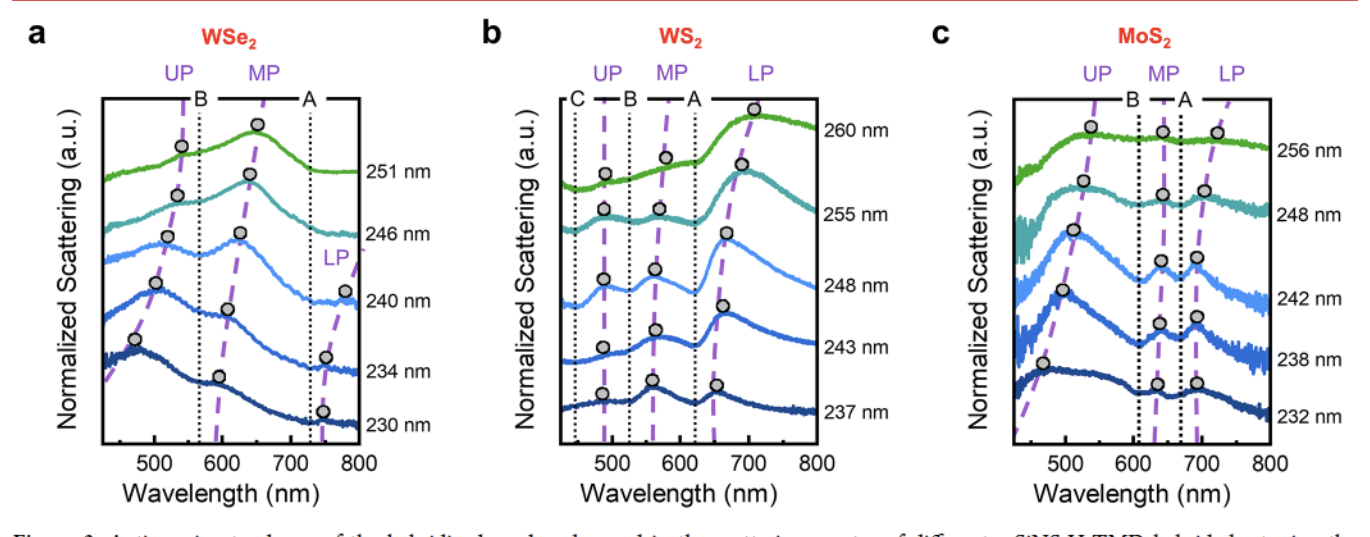


Figure 3. Anticrossing tendency of the hybridized modes observed in the scattering spectra of different a-SiNS:H-TMD hybrids by tuning the sphere sizes. The spectra are normalized and shifted for better visualization. (a) WSe₂, (b) WS₂, and (c) MoS₂ samples are all evaluated in different a-SiNS:H sizes deviating from the optimal conditions in light blue curves in the middle (the same spectra in Figure 2). The sphere diameters are listed on the right end of each spectrum. The dotted black lines mark the A, B, and C excitons. The dashed purple curves highlight the evolution of the hybridized modes, while their peak positions are labeled by the gray dots.

mapping on the right panel of Figure 1b suggests an optimal d of \sim 240 nm for broadband enhancement spanning most of the visible spectrum. Such an optimal condition happens when ED and MD are well overlapped in the interested spectrum range according to Mie theory (see Figure 1c). As for the exact 240 nm a-SiNS:Hs under study, highly spectrally overlapped ED and MD with comparable intensities are further identified experimentally through polarization-resolved scattering spectroscopy (see Materials and Methods and Figure S2 for details). The measured ED/MD spectra are presented in Figure 1c as well.

The hybridization of optical modes and TMD excitons is a collective phenomenon. Consequently, following the initial

design via single-surface-point evaluation in Figure 1b, we then consider the whole TMD area below the sphere on a substrate in Figure 1d to account for the experimental conditions (Figure S2). Through numerical simulations, we compare the performance of an optimized 240 nm a-SiNS:H (Figure 1d) with that of a 170 nm crystalline silicon nanosphere (Figure S3), whose ED and MD are also located in the visible regime. Superior performance is found for our MRI Mie resonator, with a significant global field enhancement covering the TMD monolayer (dashed lines in Figure 1d) at all visible wavelengths. Additionally, Figure 1c also suggests that a real a-SiNS:H (solid curves) may perform even better than our theoretical prediction (shaded peaks), as it offers more spectral

Nano Letters pubs.acs.org/NanoLett Letter

ED-MD overlapping.²⁴ The deviation appears because a reduced model with a constant n of ~2.1 for a-SiNS:Hs and without a substrate cannot perfectly reproduce the full spectrum.^{25–27}

In our experimental demonstrations, chemical vapor deposition (CVD)-grown TMD monolayers are transferred on a glass substrate and the designed a-SiNS:Hs with a proper dielectric function are drop-cast on the TMDs (see Figures S2c and S4). Figure 2 displays the single-particle dark-field scattering spectra of three samples: 240 nm a-SiNS:H on monolayer WSe2, 248 nm a-SiNS:H on monolayer WS2, and 242 nm a-SiNS:H on monolayer MoS2. The SEM images of the studied a-SiNS:Hs can be found in Figure S5. More details are in Materials and Methods and Figure S2a. As highlighted by the dotted lines, distinct dips are located at the energies of A and B excitons, agreeing well with the reported values. 2-9 In Figure 2b, a dip for the WS2 C exciton is also recognizable at a shorter wavelength. Compared to bare a-SiNS:H scattering (Figure 1c), multi-Rabi splittings are clearly identified as new peaks marked by the dash-dotted lines, revealing the possible formation of multiple exciton-polaritons.

Measuring a series of spectra with an anticrossing feature while tuning the cavity mode energy is one of the common methods to confirm the SC nature. 30 In single-particle experiments, this is usually achieved by using nanoparticles of different dimensions. ^{31,32} As shown in Figure 3, we experimentally evaluate the evolution of the polariton-like hybridized modes in different TMD samples by tuning the a-SiNS:H sizes away from the optimal conditions in Figure 2. A clear anticrossing tendency is observed in both WSe2 (Figure 3a) and MoS₂ (Figure 3c) samples. As for WS₂ samples (Figure 3b), the anticrossing feature of LP is also well identified while the peak position of UP barely changes due to the existence of C exciton spectrally close to B exciton. The shorter wavelength spectrum beyond the C exciton is inaccessible with our setups. The results in Figure 3 serve as important experimental evidence to support the SC nature in our system. Meanwhile, it is worth noting that the coupling strengths decrease rapidly, and the Rabi-splitting features are vanishing when the a-SiNS:H size deviates from the optimal condition by only ~ 10 nm. This is because our platform relies on the overlapped ED and MD, whose performance is very sensitive to the a-SiNS:H size. Therefore, we focus on the optimal a-SiNS:H sizes with the strongest coupling strength in Figure 2 in the following content.

In order to better confirm the physical origin of the polariton-like peaks in our observation, we employ the coupled mode theory (CMT) considering three excitonic (A, B, C) harmonic oscillators coupled with the Mie resonance (oscillator) to fit the measured spectra in Figure 2. Note that since our system relies on the highly overlapped ED and MD as discussed in Figure 1 and experimentally testified in Figure 3, we simplify the analysis by treating ED and MD together as a single mode based on the following reasons. First, we evaluate the contributions from ED and MD on coupling and spectral mode splitting through polarization-resolved scattering spectroscopy (see Figure S6) and find them always similar for all the a-SiNS:H-TMD samples. Second, the same kind of treatment has been successfully used to understand the coupling between dye aggregates and Cu2O nanospheres that feature overlapped ED and MD.31 In addition, we notice that ED's and MD's coupling strengths with excitonic dipoles have been quantitively compared in high-index silicon nanodisks³²

with a n of \sim 4.2, which gives a relatively small difference of \sim 13 \boxtimes . Compared to the literature, our $n\approx 2.1$ a-SiNS:Hs provide better overlapped ED and MD, satisfying the premise of our simplification. The details of CMT fittings can be found in Supporting Information Section S5.

Classical CMT fittings of the scattering spectra in Figure 2 are presented in Figure S7, but they cannot properly reproduce the measured spectra. This can be explained by the large g, as listed in Table S1, which approaches USC and implies the need of a correction to CMT. When the normalized coupling strength $\eta = g/\omega_0$ equals or exceeds 0.1, USC is reached, and some standard quantum optical approximations, such as the rotating wave approximation, are no longer valid. Another risk of using classical CMT when reaching or closely approaching the USC regime is the overestimation of coupling strengths, as is also observed in our system (see Table S1). This issue can be solved by rewriting the coupled oscillator matrix \mathbf{M} with frequency (ω) -dependent off-diagonal terms as

$$= \begin{bmatrix} \omega^2 - \omega_A^2 & i\gamma_A \omega & & & \omega_A \\ & \omega^2 - \omega_B^2 & i\gamma_B \omega & & \omega_B \\ & & \omega^2 - \omega_C^2 & i\gamma_C \omega & \omega_C \\ \omega_A & \omega_B & \omega_C & \omega^2 - \omega_{Mie}^2 & i\gamma_{Mie} \omega \end{bmatrix}$$
(1)

where ω_X (X = A, B, C) and ω_{Mie} are the coherent resonance frequencies of the excitonic and Mie modes. $_X$ (X = A, B, C) and $_{\text{Mie}}$ are the corresponding line widths (half width at half-maximum) of each mode and represent the decoherence rates (see Tables 1 and S2). g_X (X = A, B, C) is the coupling

Table 1. Mode Splitting and Coupling Strength

sample	WSe_2	WS_2	MoS_2
Effective Mie mode linewidth (meV)	434	445	436
Average of Mie mode and A and B exciton linewidths, $_{\mathrm{avg}}$ (meV)	224	205	179
Normal mode splitting at A exciton, 2gA (meV)	244	298	216
Normal mode splitting at B exciton, 2g _B (meV)	314	310	309
Normalized total splitting, $2(g_A + g_B)/2$ avg	1.25	1.48	1.46
Normalized coupling strength at A exciton, $\eta_{\rm A} = g_{\rm A}/\omega_{\rm A}$	0.073	0.074	0.058
Normalized coupling strength at B exciton, $\eta_{\rm B} = g_{\rm B}/\omega_{\rm B}$	0.072	0.065	0.077

strength with the Mie cavity at each excitonic transition. More details are given in Supporting Information Section S5. Then, CMT fittings with the USC correction are applied and presented in Figure 2, and a much better agreement is obtained. The fitted values from the corrected CMT are listed in Table 1. We compare the gain, $2(g_A + g_B)$, with the loss, 2_{avg} , and found that their ratio, $2(g_A + g_B)/2_{avg}$, is always larger than one for all three samples, safely confirming the SC nature and the formation of exciton-polaritons. More discussions on the SC system can be found in Supporting Information Section S6. The corrected fittings eventually determine a normalized coupling strength η up to 0.077, showing the potential to approach USC.

Note that the focus of this work lies in the radiative polaritons from optically active A and B excitons at the band edge (Figure 2, lower panels), while the band-nesting C exciton³³ is out of scope, since it is optically inactive³⁴ and spectrally almost inaccessible with our setups. We also give a

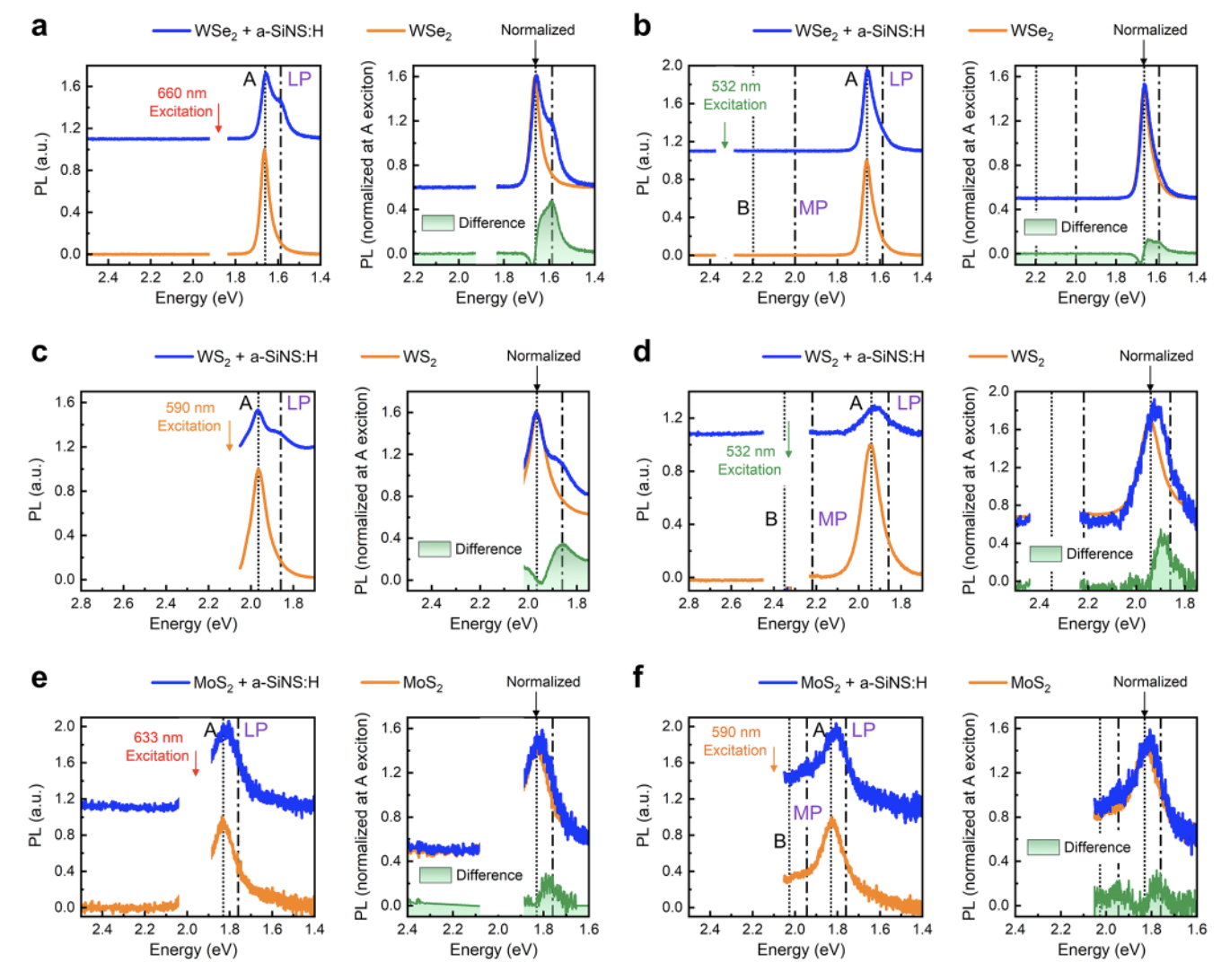


Figure 4. Robust room-temperature exciton-polariton emission in different TMD materials coupled with a broadband Mie resonator. (a, b) Left: Comparison of WSe₂ photoluminescence (PL) spectra when the well-designed a-SiNS:H is coupled (blue) and is not (orange). Right: Highlight of the exciton-polariton PL by extracting the difference between the two PL spectra after normalization. Both (a) 660 and (b) 532 nm laser excitations are tested respectively. Same as in Figure 2, the dotted lines mark the excitons and the dash-dotted lines highlight the exciton-polaritons. (c, d) Same as (a) and (b) but for the WS₂ sample and under 590 and 532 nm laser excitations, respectively. (e, f) Same as (a) and (b) but for the MoS₂ sample and under 633 and 590 nm laser excitations respectively.

rough estimate of the coupling strengths^{35,36} based on simulated field distributions in the absence of TMD monolayers (see Supporting Information Section S9 and Table S5). However, a better understanding of the system may still require more advanced models that can handle multiple oscillators.

Finally, in Figure 4, we show robust PL responses from various exciton-polaritons in different TMD samples at room temperature based on our broadband platform. It is not only another strong evidence of the SC nature but also a direct demonstration of on-demand exciton-polariton emission from the a-SiNS:H-TMD hybrids. As marked by the dash-dotted lines in Figure 4 (the same as in Figure 2), new emission lines emerge in the blue curves (for TMDs coupled with the optimized a-SiNS:Hs), as compared to the orange curves of bare TMD emission. Note that the Gaussian beam spot size (\sim 1 μ m at full width at half-maximum) for PL excitation is much larger than the a-SiNS:H cross section (\sim 240 nm in diameter), which results in up to 90 \boxtimes of the PL signal from

uncoupled TMD areas. This causes a dominant peak of the intrinsic exciton PL in all the spectra. Therefore, for better visualization, we extract the differences between the PL of coupled (blue) and bare TMDs (orange) after normalization, as illustrated in the green shaded curves in Figure 4. The remaining peaks of the differential spectra all match perfectly with the polariton peak wavelengths in the corresponding scattering spectra in Figure 2 according to the dash-dotted lines. In Figure S8, we further draw scattering and PL spectra together, which illustrates the polariton emission lines more clearly.

Since the energy differences between the observed LP emission and A excitons are 73.8, 120.6, and 55.2 meV for WSe₂, WS₂, and MoS₂ samples, respectively, much larger than the energy differences between their neutral and charged excitonic states, the influence of charge transfer can be safely excluded. In order to exclude the strain-induced effect that may be introduced by nanospheres, we also measure the PL spectra of WSe₂ coupled with a-SiNS:Hs of different sizes deviating

from the optimal value, as shown in Figure S9. WSe $_2$ is chosen from the TMDs used in this study because of its strongest polaritonic emission signal. Interestingly, with only $\sim \! 10$ nm size deviation, the emerging polariton emission line totally disappears. This not only excludes the strain-induced effect but also suggests that robust room-temperature polariton emission can only be observed in sufficiently strong SC conditions, i.e., as what we demonstrated with our broadband enhancement platform.

Besides the universal applicability to various 2D TMD polariton emission, our SC platform also provides new opportunities for excitation-wavelength-dependent control experiments to explore the decay properties of different 2D polaritonic states. Specifically, (1) multiple exciton-polaritons coexist in one system thanks to our broadband platform; (2) mode splittings up to 314 meV (or 107 nm in wavelength difference) make it easier to selectively excite the interested polaritonic states. For example, for the WSe₂ sample, we can choose a 660 nm laser to excite the lowest-energy (1.59 eV) polariton only (Figure 4a) and use another 532 nm excitation laser closer to the 2.01 eV polariton for comparison (Figure 4b). Although it is only an initial demonstration, we already observe some interesting phenomena. For both WSe2 and WS2 (Figure 4a-d), the lowest-energy polariton, LP, is found to be highly radiative, whereas the polaritonic branch between A and B excitons, MP, is nonradiative. In addition, when excited by photons with higher energies than MP, LP emission is still observed but with a significantly decreased intensity, which suggests certain amounts of energy are being dissipated through the MP state, which nonetheless is nonradiative. Interestingly, as for MoS₂ sample, divergent results are observed with LP and MP both radiative, as shown in Figure 4e,f. When we excite the MP at a close wavelength of 590 nm (Figure 4f), the comparable PL intensities of MP and LP indicate that the radiative depopulation of MP is fast enough to compete with polariton-polariton interactions.

We hypothesize that the different intrinsic A and B exciton decay properties in various TMDs are responsible for our observation. As illustrated at the lower panels of Figure 2, WSe₂ and WS₂ have a much larger energy difference between A and B excitons (ΔE_{AB}) than MoS₂ does. This makes the nonradiative decay from the B exciton to the A exciton energetically favored in WSe2 and WS2, which is expected to be a subpicosecond process.³⁷ As commonly reported, ¹/_{13,14,33,37} B excitons are nonradiative in WSe2 and WS2 but radiative in MoS₂, the same as the behaviors of MP here. Therefrom, 2D exciton-polariton decays in monolayer TMDs may be intrinsically determined by the inherent excitonic properties. Surprisingly, this assumption can explain the majority of the previous reports for not only WSe₂, WS₂, MoS₂ but also a broader library of different TMDs.^{2,4–8,38} This finding may also lead to effective modulation of polaritonic/bosonic condensation radiation through the control of inherent TMD excitonic properties, e.g., electrically. A systematic study with another blue laser to excite a third higher energy polariton would bring more insights into this exciting topic, which can be implemented in our broadband platform as well but is beyond the scope of this work.

In conclusion, we have proposed a subwavelength SC platform for broadband strong light-matter interactions with wide-ranging 2D TMDs, taking advantage of MRI Mie resonators that support spectrally overlapped ED and MD. By coupling well-designed a-SiNS:Hs with different TMDs, we

have demonstrated robust exciton-polariton emission and multi-Rabi splittings at room temperature. Our a-SiNS:H-TMD hybrid system offers new opportunities for studying cavity QED, TMD-based active polaritonics, many-body effects, and excitonic physics. As a demonstration, we applied our platform to exploring the radiative/nonradiative decay properties of different exciton-polaritons in various TMD materials. A close connection between polaritonic decays and the dynamics of their mother exciton states is found, inspiring new routes to harnessing 2D polaritonic/bosonic condensation radiations. Meanwhile, we note absorption measurements have been suggested for discriminating SC, 39 which are difficult for our single-particle configuration 40 but should be considered when available. In addition, since our single-particle configuration already shows the potential to approach the USC regime, an MRI Mie-resonant dielectric metasurface collectively coupling more excitons⁴¹ may give access to full USC in 2D TMDs, a totally new opportunity with extended possibilities in nanophotonics and quantum optics.

ASSOCIATED CONTENT

Supporting Information

The Supporting Information is available free of charge at https://pubs.acs.org/doi/10.1021/acs.nanolett.3c02540.

Materials and methods including synthesis of a-SiNS:Hs, preparation of monolayer TMDs, optical setup and measurements, and spectra fittings; characterization of a-SiNS:Hs and monolayer TMDs, Mie theory, COMSOL simulations, CMT fittings and USC correction, mode splittings, characterization of MD and ED modes, and estimation of coupling strengths based on simulations; Figures S1–S10; Tables S1–S5 (PDF)

AUTHOR INFORMATION

Corresponding Author

Yuebing Zheng — Walker Department of Mechanical Engineering and Texas Materials Institute. The University of Texas at Austin. Austin. Texas 78712. United States; Orcid.org/0000-0002-9168-9477; Email: zheng@austin.utexas.edu

Authors

Jie Fang — Walker Department of Mechanical Engineering and Texas Materials Institute. The University of Texas at Austin. Austin. Texas 78712. United States; oocid.org/0000-0002-0793-9323

Kan Yao — Walker Department of Mechanical Engineering and Texas Materials Institute. The University of Texas at Austin. Austin. Texas 78712. United States; orcid.org/0000-0002-9144-2618

Mingsong Wang — Photonics Initiative. Advanced Science Research Center. City University of New York. New York. New York 10031. United States; ocid.org/0000-0001-9071-5517

Zhuohang Yu — Department of Materials Science and Engineering. Department of Physics. Department of Chemistry. and Center for 2-Dimensional and Layered Materials. The Pennsylvania State University. University Park. Pennsylvania 16802. United States

Tianyi Zhang — Department of Materials Science and Engineering. Department of Physics. Department of Chemistry. and Center for 2-Dimensional and Layered

- Materials. The Pennsylvania State University. University Park. Pennsylvania 16802. United States
- Taizhi Jiang McKetta Department of Chemical Engineering. The University of Texas at Austin. Austin. Texas 78712. United States; o orcid.org/0000-0003-1995-6187
- Suichu Huang Walker Department of Mechanical
 Engineering and Texas Materials Institute. The University of
 Texas at Austin. Austin. Texas 78712. United States; School
 of Mechatronics Engineering. Harbin Institute of Technology.
 Harbin 150001. China
- Brian A. Korgel McKetta Department of Chemical Engineering. The University of Texas at Austin. Austin. Texas 78712. United States; o orcid.org/0000-0001-6242-7526
- Mauricio Terrones Department of Materials Science and Engineering. Department of Physics. Department of Chemistry. and Center for 2-Dimensional and Layered Materials. The Pennsylvania State University. University Park. Pennsylvania 16802. United States; orcid.org/0000-0003-0010-2851
- Andrea Alu Photonics Initiative. Advanced Science Research Center. City University of New York. New York. New York 10031. United States; Physics Program. Graduate Center. City University of New York. New York. New York 10016. United States

Complete contact information is available at: https://pubs.acs.org/10.1021/acs.nanolett.3c02540

Author Contributions

J.F. conceived the idea and designed and performed the experiments. Y.Z. supervised the whole project. Z.Y., T.Z., and M.T. prepared the monolayer TMDs. T.J. and B.A.K. synthesized the a-SiNS:H. J.F. and K.Y. conducted the theoretical derivations and COMSOL simulations. J.F., M.W., K.Y., and S.H. analyzed the data. J.F. wrote the manuscript. All authors discussed the results and commented on the manuscript.

Notes

The authors declare no competing financial interest.

ACKNOWLEDGMENTS

J.F., K.Y., and Y.Z. acknowledge the financial support of the National Science Foundation (Grant NSF-ECCS-2001650) and the Portuguese Science and Technology FDN (Grant LOA 028, Zheng). M.W. and A.A. acknowledge the financial support of the Air Force Office of Scientific Research, the Office of Naval Research, and the Simons Foundation. Z.Y. was partially supported by Materials Research Science and Engineering Center (MRSEC), The Center for Nanoscale Science, under NSF Grant DMR-2011839. T.Z and M.T. thank the Air Force Office of Scientific Research for Grant FA9550-18-1-0072. T.J. and B.A.K. acknowledge the financial support of the Robert A. Welch Foundation (Grant F-1464) and the Center for Dynamics and Control of Materials (CDCM), Materials Research Science and Engineering Center (MRSEC) (Grant DMR-1720595).

REFERENCES

- (1) Schneider, C.; Glazov, M. M.; Korn, T.; Höfling, S.; Urbaszek, B. Two-dimensional semiconductors in the regime of strong light-matter coupling. *Nat. Commun.* 2018, *9*, 2695.
- (2) Bisht, A.; et al. Collective Strong Light-Matter Coupling in Hierarchical Microcavity-Plasmon-Exciton Systems. *Nano Lett.* 2019, 19, 189–196.

- (3) Khitrova, G.; Gibbs, H. M.; Kira, M.; Koch, S. W.; Scherer, A. Vacuum Rabi splitting in semiconductors. Nat. Phys. 2006, 2, 81–90.
- (4) Flatten, L. C.; et al. Room-temperature exciton-polaritons with two-dimensional WS₂. Sci. Rep. 2016, 6, 33134.
- (5) Wang, S.; et al. Coherent Coupling of WS₂ Monolayers with Metallic Photonic Nanostructures at Room Temperature. *Nano Lett.* 2016, 16, 4368–4374.
- (6) Zhang, L.; Gogna, R.; Burg, W.; Tutuc, E.; Deng, H. Photonic-crystal exciton-polaritons in monolayer semiconductors. *Nat. Commun.* 2018, 9, 713.
- (7) Liu, X.; et al. Strong light-matter coupling in two-dimensional atomic crystals. *Nat. Photonics* 2015, 9, 30–34.
- (8) Dufferwiel, S.; et al. Exciton-polaritons in van der Waals heterostructures embedded in tunable microcavities. Nat. Commun. 2015, 6, 8579.
- (9) Lundt, N.; et al. Room-temperature Tamm-plasmon excitonpolaritons with a WSe₂ monolayer. Nat. Commun. 2016, 7, 13328.
- (10) Dufferwiel, S.; et al. Valley-addressable polaritons in atomically thin semiconductors. *Nat. Photonics* 2017, 11, 497–501.
- (11) Emmanuele, R. P. A.; et al. Highly nonlinear trion-polaritons in a monolayer semiconductor. *Nat. Commun.* 2020, 11, 3589.
- (12) Anton-Solanas, C.; et al. Bosonic condensation of exciton-polaritons in an atomically thin crystal. *Nat. Mater.* 2021, 20, 1233–1230
- (13) Wang, G.; et al. Colloquium: Excitons in atomically thin transition metal dichalcogenides. Rev. Mod. Phys. 2018, 90, 021001.
- (14) Ramasubramaniam, A. Large excitonic effects in monolayers of molybdenum and tungsten dichalcogenides. *Phys. Rev. B* 2012, 86, 115409.
- (15) Coles, D. M.; et al. Polariton-mediated energy transfer between organic dyes in a strongly coupled optical microcavity. *Nat. Mater.* 2014, 13, 712–719.
- (16) Kuznetsov, A. I.; Miroshnichenko, A. E.; Brongersma, M. L.; Kivshar, Y. S.; Luk'yanchuk, B. Optically resonant dielectric nanostructures. *Science* 2016, 354, aag2472.
- (17) Lepeshov, S.; et al. Tunable Resonance Coupling in Single Si Nanoparticle-Monolayer WS₂ Structures. ACS Appl. Mater. Interfaces 2018, 10, 16690–16697.
- (18) Wang, H.; et al. Resonance Coupling in Heterostructures Composed of Silicon Nanosphere and Monolayer WS₂: A Magnetic-Dipole-Mediated Energy Transfer Process. *ACS Nano* 2019, 13, 1739–1750.
- (19) Wang, S.; et al. Collective Mie Exciton-Polaritons in an Atomically Thin Semiconductor. *J. Phys. Chem. C* 2020, 124, 19196—19202
- (20) Cao, S.; et al. Normal-Incidence-Excited Strong Coupling between Excitons and Symmetry-Protected Quasi-Bound States in the Continuum in Silicon Nitride-WS₂ Heterostructures at Room Temperature. *J. Phys. Chem. Lett.* 2020, 11, 4631–4638.
- (21) Xie, P.; et al. Strong coupling between excitons in a two-dimensional atomic crystal and quasibound states in the continuum in a two-dimensional all-dielectric asymmetric metasurface. *Phys. Rev. B* 2021, 104, 125446.
- (22) Hinamoto, T.; et al. Resonance Couplings in Si@MoS₂ Core-Shell Architectures. Small 2022, 18, 2200413.
- (23) Shinomiya, H.; et al. Enhanced Light Emission from Monolayer MoS₂ by Doubly Resonant Spherical Si Nanoantennas. *ACS Photonics* 2022, *9*, 1741–1747.
- (24) Kornienko, V. V.; Shaimanov, A. N.; Baryshev, A. V. Overlapping the electric and magnetic dipole resonances of a silver 2D Babinet-type metasurface: Broadband high reflectance with local field enhancement. *J. Appl. Phys.* 2019, 126, 063102.
- (25) Fang, J.; et al. Directional Modulation of Exciton Emission Using Single Dielectric Nanospheres. Adv. Mater. 2021, 33, 2007236.
- (26) Fang, J.; et al. Room-Temperature Observation of Near-Intrinsic Exciton Linewidth in Monolayer WS₂. Adv. Mater. 2022, 34, 2108721.

- (27) Wang, M.; et al. Suppressing material loss in the visible and near-infrared range for functional nanophotonics using bandgap engineering. *Nat. Commun.* 2020, 11, 5055.
- (28) Yoo, D.; et al. Ultrastrong plasmon-phonon coupling via epsilon-near-zero nanocavities. *Nat. Photonics* 2021, 15, 125–130.
- (29) Baranov, D. G.; et al. Ultrastrong coupling between nanoparticle plasmons and cavity photons at ambient conditions. *Nat. Commun.* 2020, 11, 2715.
- (30) Fang, J.; et al. Tunable Couplings of Photons with Bright and Dark Excitons in Monolayer Semiconductors on Plasmonic-Nanosphere-on-Mirror Cavities. J. Phys. Chem. C 2023, 127, 9105–9112.
- (31) Ruan, Q.; et al. Coupling between the Mie Resonances of Cu₂O Nanospheres and the Excitons of Dye Aggregates. ACS Photonics 2018, 5, 3838–3848.
- (32) Todisco, F.; et al. Magnetic and electric Mie-exciton polaritons in silicon nanodisks. *Nanophotonics* 2020, 9, 803–814.
- (33) Zhao, W.; et al. Evolution of Electronic Structure in Atomically Thin Sheets of WS₂ and WSe₂. ACS Nano 2013, 7, 791–797.
- (34) Li, Y.; Wu, X.; Liu, W.; Xu, H.; Liu, X. Revealing the interrelation between C- and A-exciton dynamics in monolayer WS $_2$ via transient absorption spectroscopy. *Appl. Phys. Lett.* **2021**, *119*, 051106.
- (35) Zheng, D.; et al. Manipulating Coherent Plasmon-Exciton Interaction in a Single Silver Nanorod on Monolayer WSe₂. *Nano Lett.* 2017, 17, 3809–3814.
- (36) Sun, J.; et al. Light-Emitting Plexciton: Exploiting Plasmon-Exciton Interaction in the Intermediate Coupling Regime. *ACS Nano* 2018, 12, 10393–10402.
- (37) McCreary, K. M.; Hanbicki, A. T.; Sivaram, S. V.; Jonker, B. T. A- and B-exciton photoluminescence intensity ratio as a measure of sample quality for transition metal dichalcogenide monolayers. *APL Materials* 2018, *6*, 111106.
- (38) Kleemann, M.-E.; et al. Strong-coupling of WSe₂ in ultracompact plasmonic nanocavities at room temperature. *Nat. Commun.* 2017, 8, 1296.
- (39) Antosiewicz, T. J.; et al. Plasmon-Exciton Interactions in a Core-Shell Geometry: From Enhanced Absorption to Strong Coupling. ACS Photonics 2014, 1, 454–463.
- (40) Olson, J.; et al. Optical characterization of single plasmonic nanoparticles. *Chem. Soc. Rev.* 2015, 44, 40–57.
- (41) Castellanos, G. W.; et al. Exciton-Polaritons with Magnetic and Electric Character in All-Dielectric Metasurfaces. ACS Photonics 2020, 7, 1226–1234.